2017 NDIA GROUND VEHICLE SYSTEMS ENGINEERING AND TECHNOLOGY SYMPOSIUM
MODELING & SIMULATION, TESTING AND VALIDATION (MSTV) TECHNICAL SESSION
AUGUST 8-10, 2017 – NOVI, MICHIGAN

EFFECT OF PRE-BENDING AND HYSTERESIS OF A METAL PLATE ON BLAST-LOADING DEFORMATION: DATA VS. NUMERICAL SIMULATION

James D. Walker, Sidney Chocron, Thomas Z. Moore, Joseph H. Bradley, Alexander J. Carpenter, Carl Weiss, Charles A. Gerlach, Donald J. Grosch, Matt Grimm
Southwest Research Institute
San Antonio, TX 78238

Victor W. Burguess
RDECOM-TARDEC
Warren, MI 48397

ABSTRACT

V-shaped hulls for vehicles, to mitigate buried blast loads, are typically formed by bending plate. Such an approach was carried out in fabricating small test articles and testing them with buried-explosive blast load in Southwest Research Institute's (SwRI) Landmine Test Fixture. During the experiments, detailed time dependent deflections were recorded over a wide area of the test article surface using the Dynamic Deformation Instrumentation System (DDIS). This information allowed detailed comparison with numerical simulations that were performed with LS-DYNA. Though in general there is good agreement on the deflection, in the specific location of the bends in the steel the agreement decreases in the lateral cross section. Computations performed with empirical blast loads developed by SwRI and by more computationally intensive ALE methods in LS-DYNA produced the same results. Computations performed in EPIC showed the same result. The metal plate was then bent numerically so that the initial plate had both hardening and residual stresses from the fabrication. When blast loaded, though the deflection reduced due to the hardening in the bends in the plate, the qualitative disagreement with the lateral cross section remains. The study then focused on the material strength model for the steel. It was observed that the difference in behavior between the experiments and the computations occurs in a region where the hull metal is unloading from its formative bend. It is argued that using a kinematic yield surface with hysteresis, rather than an isotropic one with no hysteresis as is commonly done with the Johnson-Cook model, better models the unloading and hence can better match the deformation seen in the experiments.

INTRODUCTION

One approach to mitigating the effect of buried explosives on vehicles and their occupants is through a V-shaped bottom hull. As part of work funded by TARDEC, Southwest Research Institute (SwRI) has been exploring various hull shapes. One of the hull shapes examined both computationally and experimentally is what we term a bilinear V hull. This hull shape is characterized by a bend in the center and then two symmetric bends further out, as shown in cross section in Fig. 1. Between the bends the hull plate is flat. When this hull was tested with buried soil loading, it resulted in the dynamic deformed shape shown in Figs. 2 and 3. In these figures, the red points are the experimental hull deflection taken with the DDIS system (described below) and the blue points are from a numerical simulation (also described below). Both are at the respective early-time maximum deflection. Though the centerline deflections are relatively close (Fig. 2 and center point of Fig. 3), the lateral cross section of the hull shows qualitative difference between the experiment and the numerical simulation, namely that the latter has a distinct bulge (Fig. 3). This paper's objective is to understand the origin of this difference in cross-section shape, which we believe primarily lies in the unloading behavior of the plasticity model and not in errors in the blast loading or in failing to include residual stresses and hardening that arise in the fabrication process.

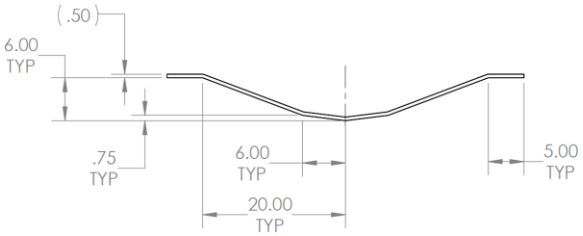

Figure 1: Side-to-side cross section drawing of the bilinear V hull (measurements in inches; 20 inches = 508 mm).

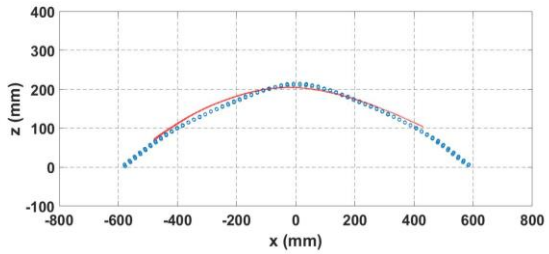

Figure 2: Front-to-back cross section comparing pre-test numerical simulation (blue) to experimental (red) dynamic shape results showing excellent agreement.

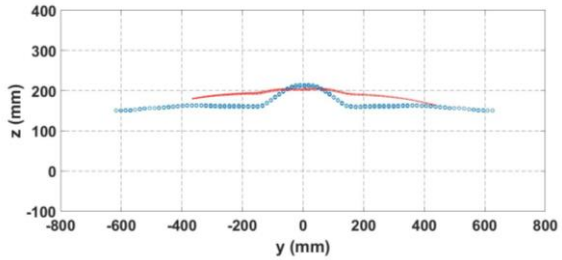

Figure 3: Side-to-side cross section comparing pre-test numerical simulation (blue) to experimental (red) dynamic shape results; good agreement at the centerline, examining the bulge is the purpose of this paper.

THE EXPERIMENTAL SETUP

In tests by Southwest Research Institute (SwRI) in support of TARDEC and the Concept Vehicle Prototype (CVP) program, explosive loading experiments were performed on the bilinear V hull component shape. Over ten of these tests were performed. Those with center blasts produced similar results. For simplicity and clarity, we focus on one of them, the first one performed (Test 1). The bilinear V hull was made of 1.27-cm-thick rolled homogeneous armor (RHA) (with 0.95-cm-thick end caps welded on) and the explosive was 1.55 kg of TNT in a cylindrical geometry with a height to diameter ratio of 0.3. The charge was buried beneath 10.16 cm of soil held in a 61-cm-diameter cardboard soil pot. The soil was a 50% clay/50% sand mixture with 12% moisture content yielding a density of 1.92 g/cm^3. The distance from the top of the soil to the bottom apex of the bilinear V hull was 25.4 cm.

As described in [1], it is now possible to gather dynamic deflection data during an explosively-loaded test event over a region of the entire hull surface. The success in collecting this wide-area data has led to a realization that the qualitative and quantitative difference between the computations and experiments is consistent from test to test and needs to be explained. The time scale of the data of interest is the first 4 milliseconds of deformation of the hull component. Using digital image correlation (DIC) software (ARAMIS) as part of the Dynamic Deformation Instrumentation System (DDIS) developed by SwRI for TARDEC, images were taken of the interior surface of a bilinear V hull every 125 microseconds. The images covered a region of the hull 80-cm across for a center cross section. Images were taken with two high-speed cameras mounted at the top of SwRI's Landmine Test Fixture (Fig. 4). Using the parallax in the cameras' optical paths, the dynamic deflection of the inside bottom of the hull during the explosive loading event was measured. LED lights illuminated a dot pattern applied to the upper surface of the inner hull; the DIC system used these, in conjunction with its calibration, to determine the physical location of the upper surface of the inner hull for each set of images that were taken during the test.

Figure 4: SwRI's Landmine Test Fixture holding a bilinear V hull component above a soil pot. At the top of the test fixture is the superstructure holding dual offset high-resolution high-speed cameras.

Figure 5 shows one frame of the movie that was produced for Test 1. The frame, at 4 milliseconds after the initial hull motion due to the blast, is at the

time of maximum deformation. The upper left part of the image colors the amount of deformation of the hull bottom, with the most deformation (colored orange) occurring directly above the explosive charge. The upper right part of the image is the deformed shape of the center side-to-side cross section at 4 milliseconds. The lower image shows the deflection of the center point, which reaches a maximum of 20.5 cm. Figure 6 then shows a sequence of images of the data, taken at 0.5 ms intervals, showing the deformation. As is seen, the blast loading essentially flattens out the bilinear V panel and moves it upwards, though the edges of the panel do not move much due to the weight of the test fixture.

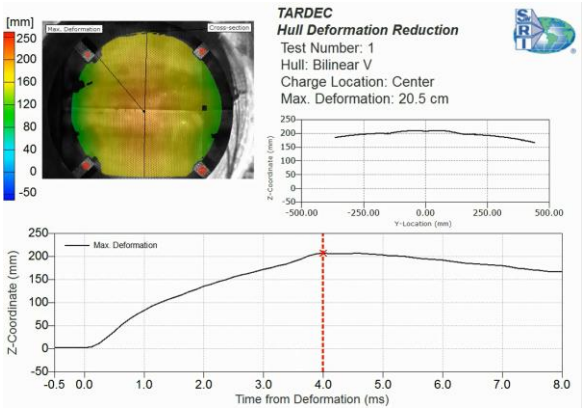

Figure 5: A frame at 4.0 milliseconds after initial hull motion from the movie showing the hull shape as seen at the inner surface.

NUMERICAL SIMULATIONS

Finite element computations were performed to examine the blast loading. The finite element models of the hull component test article panel were modeled with quad shell elements, roughly 1.55 cm by 2.0 cm (82 elements side to side and 60 elements front to back). In the first computation we present, performed before the test (referred to as the pre-test numerical simulation in the following), the finite element solver was LS-DYNA. Figure 7 shows a cross section of the fixture with the deformed blast panel at the point of maximum deflection (which according to the computation is 21.7 cm). In this paper the boundary condition has the bilinear hull V hull component welded to the test fixture. (Ref. [1] also considers a bolted configuration where the bolts could fail; this attachment scheme leads to slight differences in response, but does not affect the conclusions of paper.) Figure 8 then shows a time sequence comparison of this pre-test computation, in reverse order this time (bottom to top) from the time of first motion through 4 ms, again at 0.5 ms increments.

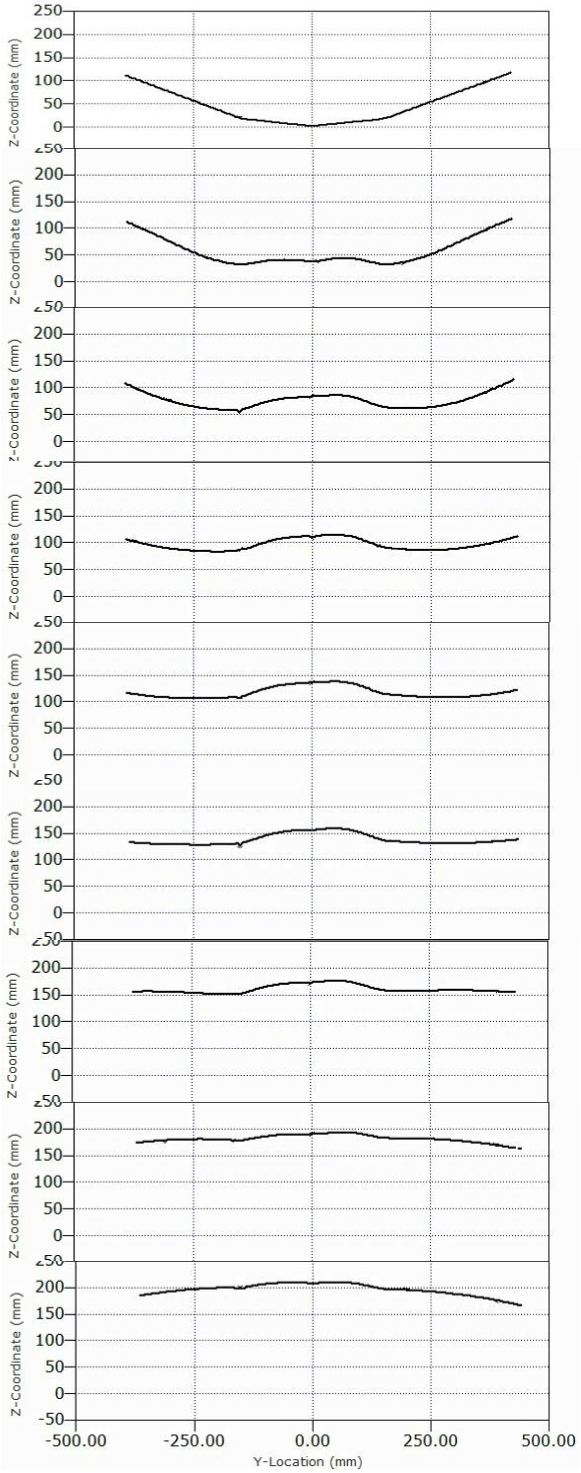

Figure 6: Sequence of frames showing the side to side cross section of the hull shape at the center from Test 1. The frames are at 0.5 ms increments from 0 to 4 ms (time increasing top to bottom).

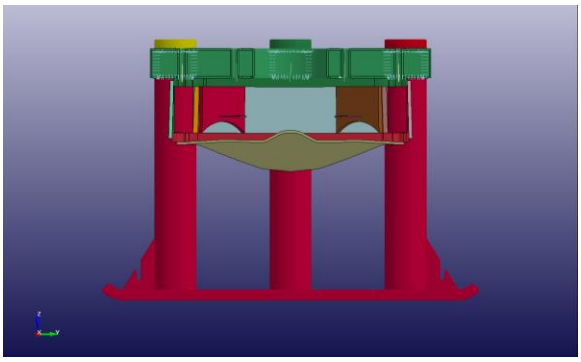

Figure 7: Pre-test numerical simulation cross section showing the maximum deformation of the panel.

Though the total centerpoint deflection of the plate agrees well with the experimental result, and the front to back deformation shape agrees well (Fig. 2), the first thought regarding the origin of the side-to-side shape discrepancy is that the blast loading may not be correct. The blast loads used in the numerical simulation presented in Figs. 7 and 8, which was performed before the experiment was conducted, were based on analytic extensions of empirical blast loads based on data collected over many years and in many test programs. The specific formulation of the loading algorithm was developed under DARPA funding for in the Adaptive Vehicle Make program [2,3]. These loads are more impulsively applied than the actual soil loads; that is, the load is applied in a shorter time frame.

Thus, the first place the authors looked to understand the origin of the difference in the cross-section-shape of the hull was in the blast loads used in the simulation. To explore the role of blast loads, two very different computations were performed. In the first, LS-DYNA was again used as the structural solver but this time the "ALE" capability was used to model the soil blast load. This approach is much more computationally intensive than the analytic empirical loads. Due to robustness issues the legs and top of the Landmine Test Fixture were removed and replaced with corresponding weights on the remaining fixture.

The second approach to performing a numerical simulation was to use the EPIC hydrocode – i.e., a completely different structural solver but using the same plate geometry and the same material models. The entire test fixture was not meshed for the EPIC computation, but the mass of the test fixture was placed into a representative mass attached to the panel edge. The blast loading approach was a Lagrangian explosive and a Lagrangian soil model where the finite elements transitioned to particles after a large amount of deformation [4]. These particles then loaded the bilinear V hull. Some images from this loading procedure are in Fig. 9.

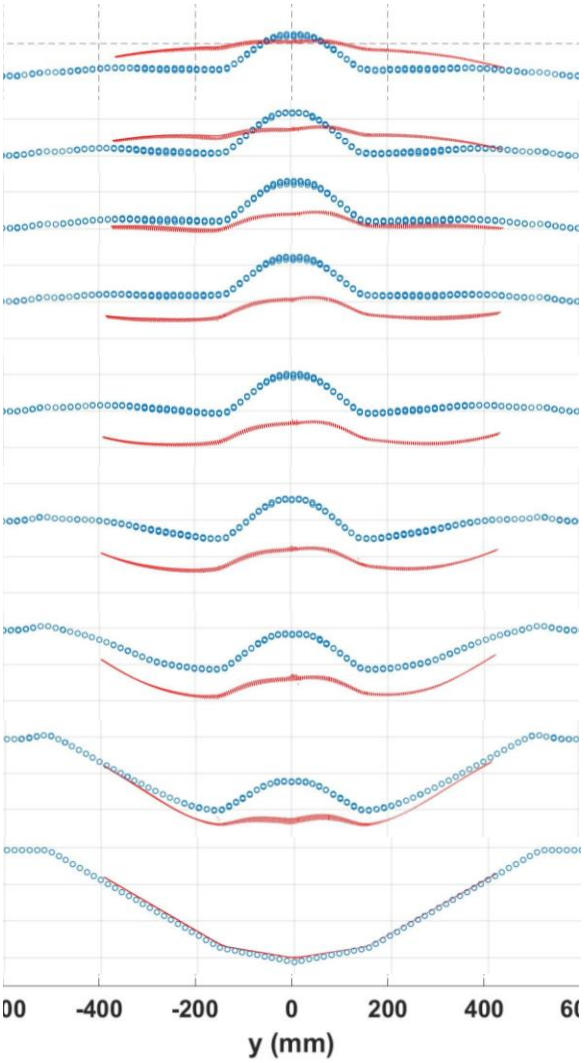

Figure 8: Frames show the pre-test numerical simulation compared with the Test 1 measured hull shape cross section from 0 to 4 ms in 0.5 ms increments (time increasing bottom to top).

The LS-DYNA ALE and EPIC models working directly with the soil and explosive produce better deflection vs. time behavior, implying that they are better at distributing the blast-loading and impulse over time. Figure 10 shows this behavior. Interestingly, however, at the time of maximum deflection, the results for all three numerical simulation approaches (LS-DYNA with analytic empirical blast loads, LS-DYNA ALE, and EPIC), produce similar side-to-side cross sections (Figure 11). Not only are they quantitatively similar in the prediction of the centerpoint deflection, but the shape of the center bulge is almost identical for all of them. Thus, we conclude that the shape of the center bulge in the numerical simulations is not due to the

blast and soil loading, or at least it is not due to any deficiency in the empirical loading approach.

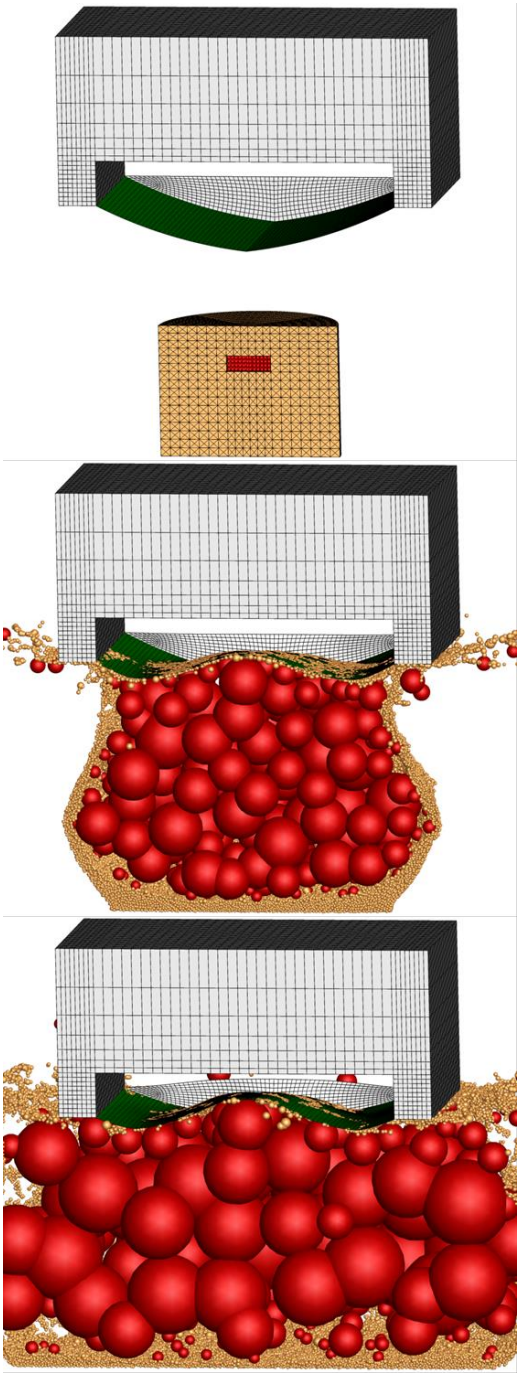

Figure 9: Images from the EPIC computation showing loading of the plate at 0, 3, and 6 ms. The red is explosive, which begins as elements and then transitions to particles as the deformation becomes large. The soil is brown, also beginning as elements and transitioning to particles as the deformation becomes large.

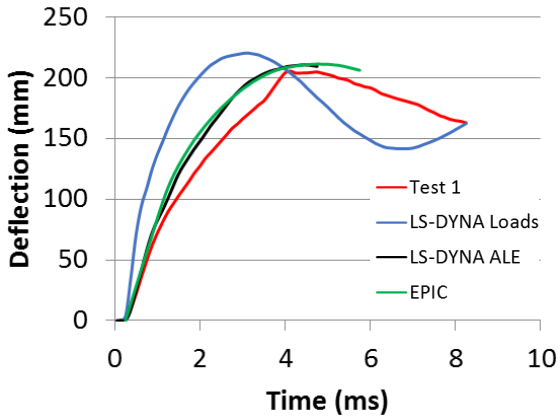

Figure 10: Centerpoint deflection history using LS-DYNA with analytic loads (blue), LS-DYNA with ALE and soil model (black), EPIC with soil model (green), and experiment (red).

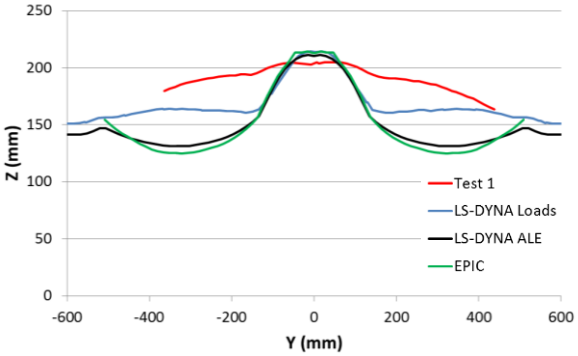

Figure 11: Comparison of the cross section shapes of the three numerical methods and the experiment, each at their respective maximum deflection time.

PRE-BENDING THE PLATE

In the numerical simulations presented above, the bilinear V hull component was modeled in such a way that at the bends there was no residual stress or work hardening of the material. This is the way these computations are typically performed – the initial material state is virgin material, and there is no consideration as to how the material arrived at the bent state.

To explore the question of whether bending the plate as part of the initialization of the blast geometry affects the numerical simulations results, within LS-DYNA a flat pate made of shell elements was taken. Boundary conditions were applied to bend the plate into the bilinear V hull shape. This hull component finite element model now had shell elements that were initialized due to the initial bend – the elements in the vicinity of the bend had both stress states and plastic strain (hence work hardening states). The bends in the shell mesh essentially occurred in one element across, Figure 12. This plate was then

attached to the test fixture and loaded with the analytic empirical blast loads.

As an aside, we mention here that the constitutive model for the RHA plate was the same in all simulations. It is a Johnson-Cook model with values taken from [5].

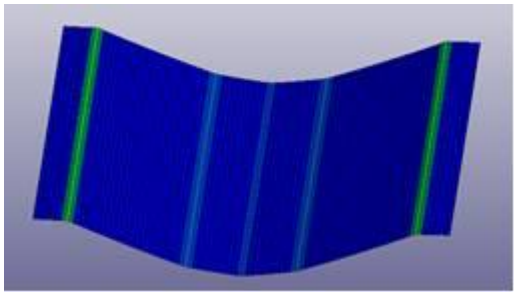

Figure 12: Equivalent plastic strain in the plate after the forming bends. The outer bend elements have 19.7% strain, the two bilinear V bends elements have 9.5% strain, and the centerline bend elements have 3.75% strain.

The result of this computation showed less deflection and deformation of the plate as would be expected since the material is now hardened in the bend region from the forming bends of the plate. However, the qualitative feature of the bulge in the center is still there. As can be seen in Fig. 13, there is little difference in the qualitative shape at the time of the maximum deflection of the plate. (There is a small 6.35 mm offset in comparison to the previous computations due to where the shell elements were identifying their position.)

This computation implies that the residual stress and strain state (including the hardening state) due to the initial forming bend is not the origin of the qualitative lack of agreement with the center bulge that is seen at late time.

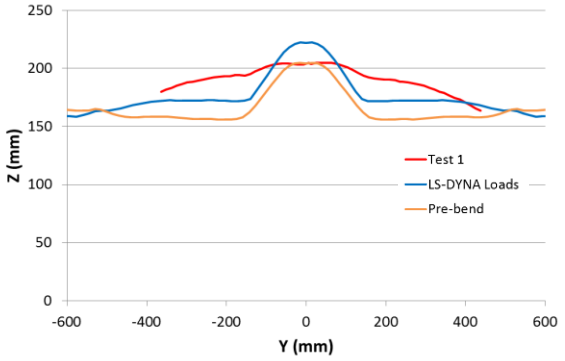

Figure 13: Maximum deflection shape of the plate in the numerical simulation which included pre-bending.

THE PLASTIC BEND AND THE ROLE OF ISOTROPIC AND KINEMATIC HARDENING

To better understand what is occurring at the bend, it will be analyzed in the context of the plate bend, though for simplicity we will not include the $1/(1-\nu^2)$ term multiplying the stress that accompanies the plate stress vs. a beam stress (ν is Poisson's ratio). It is assumed the plate is $2h$ in thickness. The centerline fiber of the plate is assumed to have constant length $X = R\theta$, as shown in Fig. 14. The outer (upper fiber in the figure) fiber is in tension. It is a constant distance h above the center fiber. It has a strain of

$$\varepsilon_+ = \frac{R_+\theta - R\theta}{R\theta} = \frac{(R+h)\theta - R\theta}{R\theta} = \frac{h\theta}{X}. \qquad (1)$$

The subscript + refers to the outer (upper) fiber. Thus, there is direct relationship between strain and the bending angle. For the rest of the discussion, however, we will work with the strain.

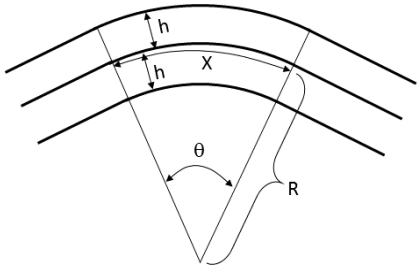

Figure 14: Geometry of the plate bend, showing the central fiber which maintains a constant length X and the outer surface (upper) fiber and inner surface (lower) fiber. The bend angle is θ and the bend radius is R.

The inner (lower) fiber is in compression and is a constant distance h below the center fiber. Its strain is $\varepsilon_- = -h\theta / X = -\varepsilon_+$. Each fiber through the thickness has its own strain and is assumed to depend linearly on the distance from the center fiber. Hence, the strain for any fiber can be written in terms of the outer fiber strain as

$$\varepsilon(y) = \varepsilon_+ \frac{y}{h}, \quad -h \le y \le h. \qquad (2)$$

In the following, the plastic strain is assumed to be close to the total strain (rigid plastic assumption) to simplify the computations.

When the plate is bent plastically, its resistance to bending is given by the moment

$$M = \int_{-h}^{h} \sigma_{xx}(y) y \, dy, \tag{3}$$

where $\sigma_{xx}(y)$ is the in-plane stress in each fiber. If the material is deforming plastically, a common model (and the one used in the above computations) is the Johnson-Cook form where

$$Y = A + B\varepsilon^n. \tag{4}$$

The specific values used in the above computations originated from 2 inch thick RHA and were A = B = 780 MPa and n = 0.106 [5]. For this analysis we are not including the strain rate (C = 0.004) and thermal softening terms (m = 1). Given the strain through the plate thickness in Eq. (2), it is possible to evaluate the moment expression in Eq (3) with $\sigma_{xx}(y) = A + B(\varepsilon(y))^n$ as

$$\frac{M}{h^2} = A + \frac{2}{n+2} B\bar{\varepsilon}_+^n. \tag{5}$$

Thus, as the joint continues to bend the moment increases and it becomes more difficult to bend because of the work hardening. If there was no work hardening, the force required to bend this plastic hinge would be independent of the current bend angle.

Now consider what happens if the bending is stopped, at an outer fiber strain of $\bar{\varepsilon}_+$, and now the plate is bent back in the other direction. First, the sign of M changes as now the roles of tension and compression exchange in the bend, with compression in the upper fibers and tension in the lower fibers. If the work hardening is isotropic, where the yield surface expands due to work hardening but stays in the same place in stress space, then the result for the moment (save for the sign) remains the same, where it is just as difficult to bend the material back as it is to continue bending it forward. In particular, for the upper fiber the stress during compression when the bending direction is reversed is

$$\sigma_+ = -(A + B(\bar{\varepsilon}_+ + |\, \bar{\varepsilon}_+ - \varepsilon_+ \,|)^n) = -A - B(2\bar{\varepsilon}_+ - \varepsilon_+)^n, \tag{6}$$

where again $\bar{\varepsilon}_+$ is the strain on the upper fiber due to the initial bend.

However, if the hardening is kinematic, meaning that the yield surface maintains its shape and size in stress space and moves in stress space to produce the hardening, then the stress terms during the unload differ from the stress terms during load. For the Johnson-Cook model, the initial yield is given by A and hence the extent of the yield surface is 2A. If it is assumed the same hardening behavior continues, then as the upper fiber goes from tension with a stress of $\sigma_+ = A + B\bar{\varepsilon}_+^n$ to compression, its new stress will be

$$\begin{aligned} \sigma_+ &= A + B\bar{\varepsilon}_+^n - (2A + B(\bar{\varepsilon}_+ + |\, \bar{\varepsilon}_+ - \varepsilon_+ \,|)^n - B\bar{\varepsilon}_+^n) \\ &= -A + 2B\bar{\varepsilon}_+^n - B(2\bar{\varepsilon}_+ - \varepsilon_+)^n. \end{aligned} \tag{7}$$

The difference in magnitude of the fiber stress in unloading for the isotropic and kinematic models is $2B\bar{\varepsilon}_+^n$, with less stress in magnitude for the kinematic hardening.

If we look at the magnitude of the moments, the stress in isotropic hardening continues to increase, and it is the same in bending both directions at the instance of the reversal of the bend. Explicitly, the moment is

$$\frac{-M}{h^2} = A + \frac{2}{n+2} B(2\bar{\varepsilon}_+ - \varepsilon_+)^n. \tag{8}$$

Right at the instant of reversing the bend, $\varepsilon_+ = \bar{\varepsilon}_+$, and the moment is

$$\frac{-M}{h^2} = A + \frac{2}{n+2} B\bar{\varepsilon}_+^{\,n}. \tag{9}$$

For the kinematic hardening the result is quite different. Integrate Eq. (3) using Eq. (7) to obtain the moment,

$$\frac{-M}{h^2} = A + \frac{2}{n+2} B\{(2\bar{\varepsilon}_+ - \varepsilon_+)^n - 2\bar{\varepsilon}_+^n\}. \tag{10}$$

This value is substantially less in magnitude than the isotropic hardening expression. Thus it is substantially easier to bend the plate back. Right at the instant of changing bend direction, the moment to bend in the opposite direction is

$$\frac{-M}{h^2} = A - \frac{2}{n+2} B\bar{\varepsilon}_+^n. \tag{11}$$

Figure 15 graphs the moments for forward bend and then reverse bend after the forward bend. As can be seen, the hysteresis in the kinematic yield surface leads to a large hysteresis in the bending resistance. Of course, this is for a highly idealized kinematic hardening model, but it exhibits that kinematic hardening does produce different bend resistances when bending in different directions.

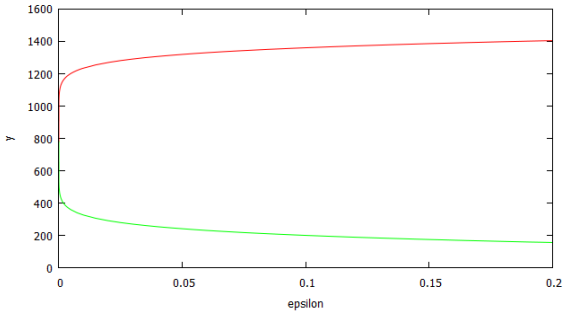

Figure 15: Bending moment (resistance) vs. strain. The upper curve shows the initial bend. The initial bending moment after reversal of the bend direction for isotropic hardening overlays this curve. The lower curve is the magnitude of the initial bending resistance for the reverse direction in the case of kinematic hardening.

THE ANGLE HISTORY

It is difficult to exactly compute an angle in the vicinity of the initial bend in the bilinear V hull due to the curvature of the bend. However, Fig. 16 shows approximately what this deformation is vs. time for the experiment and for the pre-test numerical simulation (the analytic empirical loads model with the virgin-state plate). It is seen that in the experiment, the angle increases at early time from an initial angle of 15° to an angle of 20°, and then it decreases over time to a final angle of less than 10°. Thus, the plate initially bends in a direction that continues the load path of the forming process and then the subsequent deformation is unloading. For the numerical simulation, there is an early bending from 15° to 30°, and then it essentially holds steady for the rest of the computation, showing large resistance to unloading. Thus, the unloading does not occur and the angle does not decrease, even though it is likely that the loads are such that unloading should occur.

Our conclusion is that the central feature of the cross-section deformed shaped that does not agree with the experiment is due to the current handling of unloading in the plasticity model. If kinematic hardening were employed, rather than isotropic hardening, we would expect to see unloading and thus a decrease in the size of this bulge in the center.

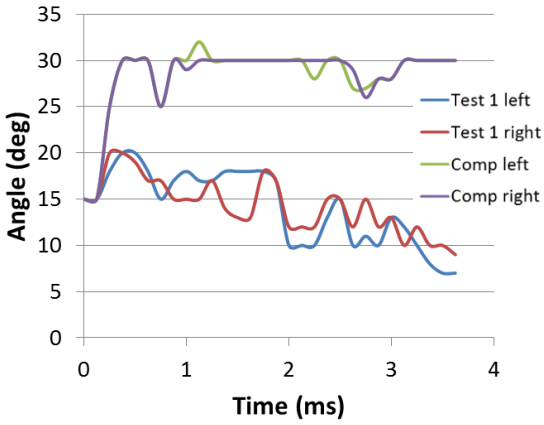

Figure 16: Approximate bend angle vs. time from initial motion for the two off-center bilinear-V bends.

The Johnson-Cook model is an isotropic hardening model. Unfortunately, there is not a kinematic hardening model within LS-DYNA that has a similar stress strain curve. The authors did, however, perform some computations with a kinematic model in the code. It allowed a linear-hardening yield surface which, unfortunately, did not allow a good match to the Johnson-Cook model. Specific values used were A = 780 MPa as in the Johnson Cook model, B = 7.8 GPa, and n = 1 (i.e., linear). Though these curves are not very similar, they match at the initial yield and at a strain of 7.6% at a stress of 1.37 GPa.

Results of computations with this plasticity model are shown in Fig. 17. These computations pre-bent the plate and used the empirical loads. There is surprising agreement between the Johnson-Cook model computation and the linear-hardening yield surface when run with isotropic hardening. In particular, the central bulge behavior is maintained. However, when run in a kinematic hardening mode, the maximum deflected shape is quite different. The bulge is flatter, which is the main point to emphasize with Fig. 17, showing that unloading does allow some flattening of the central bulge. The max deflection is much larger, in part due to the large unloading rotation of the plate where it is attached to the test fixture. We do not have dynamic data for the angle of this attachment, but static post-test analysis show the angle is relatively flat. These constitutive model constants are not good constants for RHA, but the kinematic hardening behavior feature does show unloading bending not seen with the isotropic model, which implies that it would have less of a plastic bulge feature.

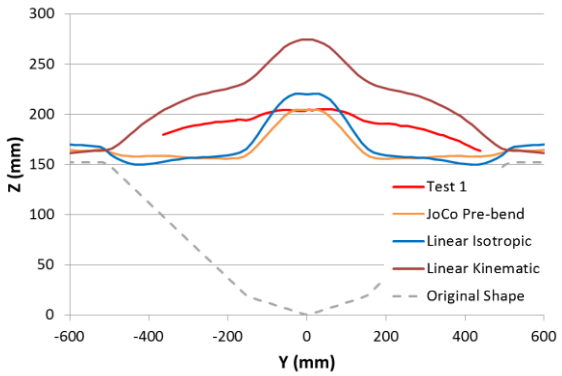

Figure 17: Results of numerically pre-bent plates with the Johnson-Cook model (which has isotropic hardening), and the linear hardening model in both an isotropic and kinematic hardening mode.

CONCLUSION

It was shown that a lack of agreement in the side-to-side cross section deformation of the blast-driven maximum deflection of the bilinear V hull is not due to blast-loading approaches or the initial hardening due to the forming of the plate. Rather, it is likely due to the constitutive model used in the simulations not correctly handling the plastic response and in particular the hysteresis observed upon unloading, though more work needs to be performed to accurately model the plate deformation.

ACKNOWLEDGMENTS

The experiments and initial analysis were funded by TARDEC through a National Advanced Mobility Consortium Other Transaction Agreement for the Hull Deformation Reduction program. The subsequent analysis of the effect of the pre-bend state of the material and the effect of plasticity hysteresis was funded by Southwest Research Institute.

Disclaimer: Reference herein to any specific commercial company, product, process or service by trade name, trademark, manufacture, or otherwise, does not necessarily constitute or imply its endorsement, recommendation, or favoring by the United States Government or the Department of the Army (DoA). The opinions of the authors expressed herein do not necessarily state or reflect those of the United States Government or the DoA, and shall not be used for advertising or product endorsement purposes.

REFERENCES

[1] J. D. Walker, D. J. Grosch, S. Chocron, M. Grimm, A. J. Carpenter, T. Z. Moore, C. Weiss, R. P. Bigger, J. T. Mathis, K. McLoud, "Direct Comparison of Wide-area Hull Deformation from Dynamic Measurement during Blast vs. Numerical Simulation," NDIA GVSETS, Novi, Michigan, August 3-5, 2016.

[2] S. A. Mullin, A. J. Carpenter, J. P. Riegel, III, P. A. Cox, J. M. McFarland, C. Weiss, J. D. Walker, D. S. Riha, D. J. Grosch, J. T. Mathis, "New Analytical Formulations for Land Mine Total and Specific Impulse Predictions," Proc. 28th Int. Symp. on Ballistics, Atlanta, Georgia, September 23 – 26, 2014.

[3] J. D. Walker, S. Chocron, M. S. Moore, G. C. Willden, "Blast and Ballistic Survivability Analysis Tools for Design Optimization Developed in DARPA's Adaptive Vehicle Make (AVM)," NDIA GVSETS, Novi, Michigan, August 4–6, 2015.

[4] G. R. Johnson, S. R. Beissel, C. A. Gerlach, K. T. Danielson, R. J. Moral, J. L. O'Daniel, "Lagrangian computational approaches for buried explosive charges involving explosive-soil-structure-air interactions and fragmentation," manuscript, 2016.

[5] H. W. Meyer, Jr., D. S. Kleponis, "An Analysis of Parameters for the Johnson-Cook Strength Model for 2-in Thick Rolled Homogeneous Armor," ARL-TR-2528, Aberdeen, Maryland, 2001.